

Chemical Science

Accepted Manuscript

This article can be cited before page numbers have been issued, to do this please use: C. Coperet, L. S. Rochlitz, K. Searles, J. Alfke, D. Zemlyanov and O. V. Safonova, *Chem. Sci.*, 2020, DOI: 10.1039/C9SC05599A.



This is an Accepted Manuscript, which has been through the Royal Society of Chemistry peer review process and has been accepted for publication.

Accepted Manuscripts are published online shortly after acceptance, before technical editing, formatting and proof reading. Using this free service, authors can make their results available to the community, in citable form, before we publish the edited article. We will replace this Accepted Manuscript with the edited and formatted Advance Article as soon as it is available.

You can find more information about Accepted Manuscripts in the [Information for Authors](#).

Please note that technical editing may introduce minor changes to the text and/or graphics, which may alter content. The journal's standard [Terms & Conditions](#) and the [Ethical guidelines](#) still apply. In no event shall the Royal Society of Chemistry be held responsible for any errors or omissions in this Accepted Manuscript or any consequences arising from the use of any information it contains.

Journal Name

ARTICLE

Silica-Supported, Narrowly Distributed, Subnanometric PtZn Particles from Single Sites with High Propane-Dehydrogenation Performance^a

Lukas Rochlitz,^a Keith Searles,^a Jan Alfke,^{a, c} Dmitry Zemlyanov,^b Olga V. Safonova,^c Christophe Copéret^{*a}

Received 00th January 20xx,
Accepted 00th January 20xx

DOI: 10.1039/x0xx00000x

www.rsc.org/

The development of highly productive, selective and stable propane dehydrogenation catalysts for propene production is strategic due to the increasing need for propene and the availability of shale gas, an abundant source of light alkanes. In that context, the combination of surface organometallic chemistry (SOMC) and thermolytic molecular precursor (TMP) approach is used to prepare bimetallic subnanometric and narrowly distributed Pt-Zn alloyed particles supported on silica via grafting of a Pt precursor on surface OH groups present in a Zn single-site containing material followed by a H₂ reduction treatment. This material, that exhibits a Zn to Pt molar ratio of 3:2 in the form of alloyed PtZn particles with a 0.2 to 0.4 fraction of the overall Zn amount remaining as Zn^{II} sites on the silica surface, catalyzes propane dehydrogenation (PDH) with high productivity (703 g_{C₃H₆} g_{Pt}⁻¹ h⁻¹ to 375 g_{C₃H₆} g_{Pt}⁻¹ h⁻¹) and very low deactivation rates (*k_d* = 0.027 h⁻¹) over 30 h at high WHSV (75 h⁻¹). This study demonstrates how SOMC can provide access to highly efficient and tailored catalysts through the stepwise introduction of specific elements *via* grafting to generate small, homogeneously and narrowly distributed supported alloyed nanoparticles at controlled interfaces.

Introduction

Propene is the second most utilized building block of the petrochemical industry besides ethene, and its production has been dramatically influenced by the emergence of shale gas resources. Indeed, crackers have been converted from naphtha to ethane units, with ethane feedstocks predominantly producing ethene, thereby reducing propene production. To compensate for the resulting propene production gap, the development of on-purpose propene production technologies has thus been on the rise.^{1,2} The most used on-purpose technology is selective propane dehydrogenation (PDH), a highly energy intensive process ($\Delta H_{298}^0 = 124.3 \text{ kJ mol}^{-1}$), industrially implemented mainly *via* two processes using a bimetallic Pt-Sn/Al₂O₃ (UOP Oleflex process) or a metal-oxide based Cr₂O₃/Al₂O₃ (Lummus Catofin process) catalyst.³ Due to the requirement of high reaction temperatures (500 – 700 °C) to reach reasonable conversion levels, one of the biggest issues for the existing systems is catalyst stability due to coke formation and sintering requiring constant and rapid regeneration.³ The development and understanding of catalytic systems with increased stability while keeping a high selectivity

and productivity is thus an intense field of research. In particular, major research endeavors focused on bi- and multi-metallic systems related to the industrial Pt-Sn/Al₂O₃ catalyst. In all cases, a combination of Pt with a second metal (In, Sn, Ga, Cu, Zn, etc.) beneficially influenced the catalyst performance as compared to monometallic Pt catalysts.^{4–9} While the selectivity for most of the systems reaches high levels, all of them suffer from deactivation. Zn, a highly abundant and non-toxic metal, is of special interest as the second component in bimetallic systems for PDH but has been studied less extensively when compared to more prominent post-transition-metals Sn and Ga.^{3,10}

Most synthetic strategies for bimetallic Pt-Zn dehydrogenation catalysts rely on well-established impregnation techniques.^{9,11,12} While being simple catalyst preparation methods, impregnation techniques typically yield poorly defined systems with inhomogeneous distribution of the components due to complex dissolution/precipitation events that occur in aqueous conditions. In order to develop more controlled preparation methods, surface organometallic chemistry (SOMC)^{13–15} in combination with the thermolytic molecular precursor approach (TMP)^{16,17} has emerged as a powerful preparation technique. In particular, it has been shown that supported single-sites can be used as building blocks to generate supported nanoparticles with controlled interfaces, allowing the introduction of dopants at the interface between silica and the metal particles or alternatively yielding a bimetallic alloy supported on SiO₂.^{17–20} A Pt-Ga alloy prepared through this approach displays high productivity and stability in

^a Department of Chemistry and Applied Biosciences, ETH Zürich, Vladimir-Prelog-Weg 1-5, CH-8093 Zürich, Switzerland

^b Birck Nanotechnology Center, Purdue University, 1205 West State Street, West Lafayette, Indiana 47907, United States

^c Paul Scherrer Institut, CH-5232 Villigen, Switzerland

*Electronic Supplementary Information (ESI) available: Experimental details, material characterization data, catalytic measurement details



the PDH reaction that has been attributed to surface dilution of Pt upon the introduction of gallium.²¹

In view of the known activity of PtZn in PDH and improved performance of catalysts prepared via SOMC/TMP approach, we reason that SOMC could constitute an ideal way to generate small and narrowly dispersed PtZn alloys by first installing Zn^{II} single sites on a SiO₂ support followed by anchoring of a Pt precursor on the Zn^{II}/SiO₂ material and a subsequent treatment under H₂ to generate the desired particles. These silica-supported PtZn nanoparticles were characterized by a multi-technique approach (CO and pyridine adsorption FTIR as well as X-ray photoelectron spectroscopy (XPS) and X-ray absorption spectroscopy (XAS) studies); they show high productivity (703 g_{C3H6}/ (g_{Pt} h)), high selectivity (≥ 95 %) and an outstanding stability (*k_d* = 0.027) at high WHSV compared to other Pt-Zn based systems for PDH at 550 °C. This improved performance is attributed to the formation of subnanometric and narrowly distributed alloyed particles supported on Zn^{II} modified silica that likely plays a role in stabilizing these particles under PDH reaction conditions.

Results and Discussion

The bimetallic Pt-Zn system was prepared *via* SOMC in a three-step process involving first the generation of Zn single-sites, then grafting of Pt(II) molecular precursor onto regenerated OH groups followed by a hydrogen treatment. Grafting of [Zn(OSi(OtBu)₃)₂]₂ on SiO₂₋₇₀₀ followed by a thermal treatment at 600 °C yielded Zn^{II}/SiO₂ as a white solid that contains Zn^{II} single sites (1.73 wt% Zn – 0.80 Zn/nm²), free of organic ligands along with isolated OH sites (0.66 OH/nm²)

(Figure 1 (a)).^{22,23} In the next step, [Pt(OSi(OtBu)₃)₂](COD) (1.2 equiv/OH)^{24,25} (COD = 1,5-cyclooctadiene) was grafted onto the surface OH groups of Zn^{II}/SiO₂; the resulting supernatant contained [Pt(OSi(OtBu)₃)₂](COD) (0.35 equiv Pt_{added}⁻¹) and HOSi(OtBu)₃ (0.35 equiv Pt_{added}⁻¹). The obtained white material – Pt(OSi(OtBu)₃)₂(COD)Zn^{II}/SiO₂ – dried under high vacuum (10⁻⁵ mbar) contained 2.90 wt% Pt, 1.62 wt% Zn (1.66 equiv Pt⁻¹), 4.44 wt% C (24.9 equiv Pt⁻¹) and 0.79 wt% H (52.7 equiv Pt⁻¹). The too high C and H values (20 C and 39 H expected) can be explained by a chemisorption (coordination) of some of the released HOSi(OtBu)₃ – formed during grafting of the Pt precursor – on the silica-support containing Zn^{II} Lewis acid sites. This is evidenced by the low amount of observed HOSi(OtBu)₃ released in solution compared to amount of remaining [Pt(OSi(OtBu)₃)₂](COD)), revealing that 45 % of the expected HOSi(OtBu)₃ is missing and remains chemisorbed at the surface of the support consistent with the elemental analysis. The IR spectrum revealed only partial consumption of the surface OH groups compared to Zn^{II}/SiO₂. This process is accompanied by the appearance of ν(C-H) at 3000–2800 cm⁻¹ and δ(C-H) at 1500–1340 cm⁻¹ (Figure 1 (b) and supporting information Figure S3). All these data are consistent with grafting of the Pt^{II} precursor through surface OH groups and the retention of some silanol on the surface. Furthermore, solid-state NMR supports the formation of ≡SiOPt(OSi(OtBu)₃)₂(COD) with signals at 1.5 ppm and 5.0 ppm in ¹H SSNMR and signals at 30 ppm and 91 ppm in the ¹³C SSNMR spectrum, respectively (supporting information Figures S4 and S5). The data is consistent with the formation of a grafted Pt^{II} complex together with Zn single-sites in Pt(OSi(OtBu)₃)₂(COD)Zn^{II}/SiO₂. The material was subsequently treated under H₂ at 600 °C for 8 h yielding a black material -

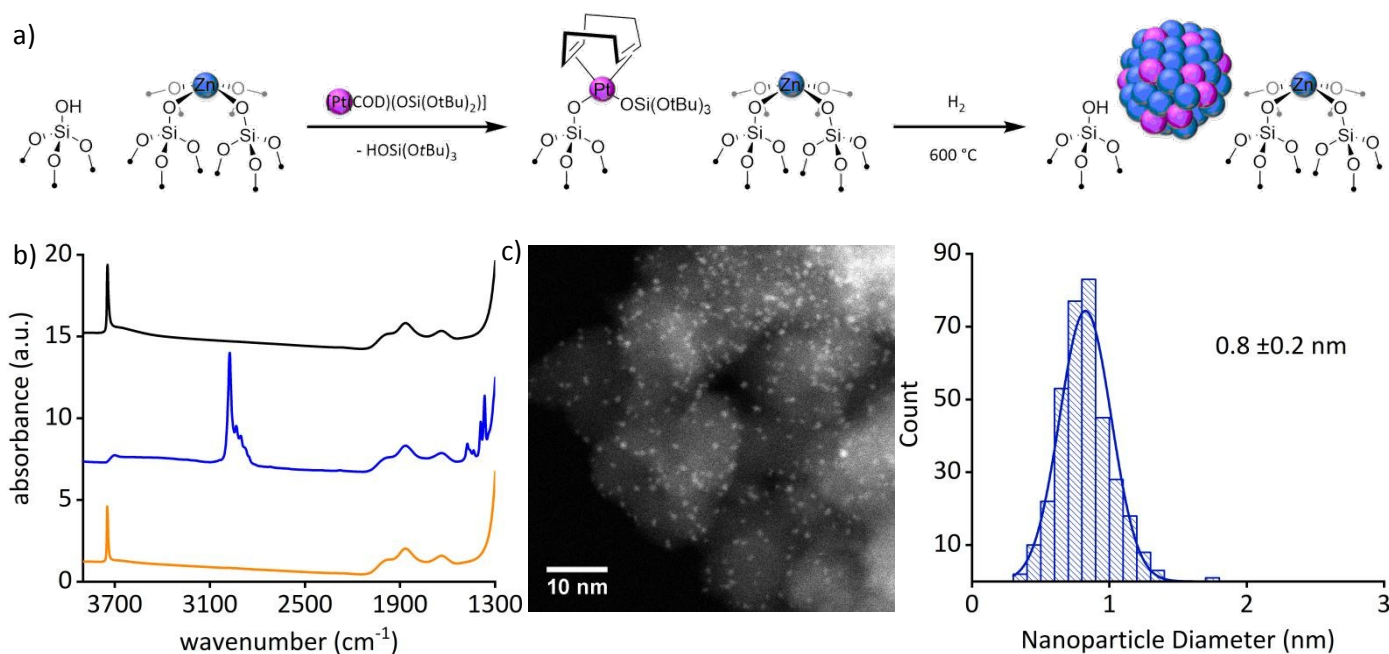
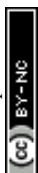


Figure 1. (a) Schematic representation of the synthesis of the material Pt⁰Zn⁶⁺/SiO₂. (b) FTIR spectra of Zn^{II}/SiO₂ (orange), Pt(OSi(OtBu)₃)₂(COD)Zn^{II}/SiO₂ (blue) and Pt⁰Zn⁶⁺/SiO₂ (black). (c) Representative HAADF-STEM image and particle size distribution of Pt⁰Zn⁶⁺/SiO₂.



Pt⁰Zn^{δ+}/SiO₂ - suggesting the formation of particles (3.05 wt% Pt, 1.54 wt% Zn). HAADF-STEM images of **Pt⁰Zn^{δ+}/SiO₂** confirmed the formation of well-dispersed and narrowly distributed sub-nanometric particles (0.8±0.2 nm) (Figure 1 (c)).

cm⁻¹) and Zn^{II} sites that are likely to be in close proximity to the alloyed particles. Another band at 1906 cm⁻¹ not observable for **Pt⁰/SiO₂** – is consistent with a μ₂-binding mode of CO on the **Pt⁰Zn^{δ+}/SiO₂** material. In addition to the CO IR studies, pyridine

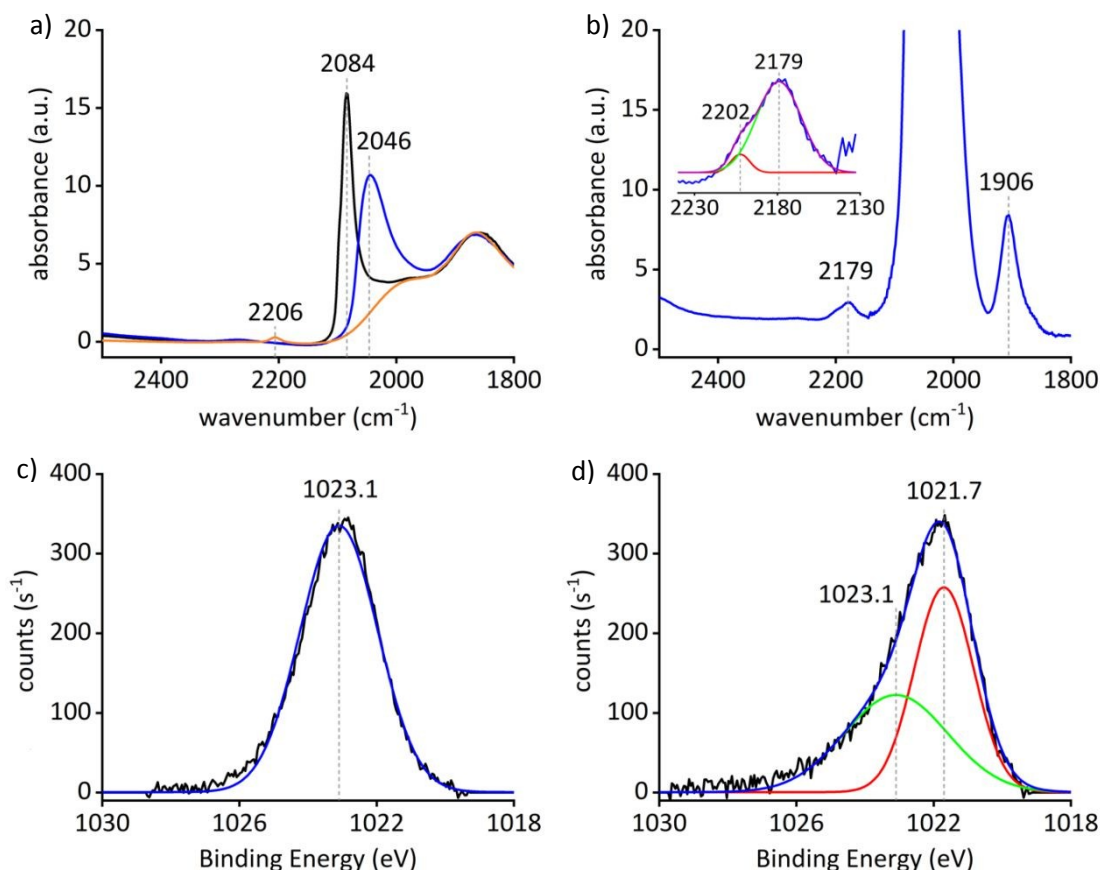


Figure 2. (a) CO adsorption on **Pt⁰/SiO₂** (black), **Zn^{II}/SiO₂** (orange) and **Pt⁰Zn^{δ+}/SiO₂** (blue). The spectra are normalized to the ν_{SiO} vibrational frequency at 1865 cm⁻¹. (b) Background subtracted spectrum of CO adsorption on **Pt⁰Zn^{δ+}/SiO₂** (blue) and two component Gaussian fit (red, green; cumulative fit (purple)) of the CO adsorption region around 2179 cm⁻¹ of **Pt⁰Zn^{δ+}/SiO₂**. (c) High resolution Zn 2p_{3/2} XPS spectrum of **Zn^{II}/SiO₂** (black) and Gaussian-Lorentzian fit to the data (blue). (d) High resolution Zn 2p_{3/2} XPS spectrum for **Pt⁰Zn^{δ+}/SiO₂** (black), two component Gaussian-Lorentzian fit to the data (green: 45%; red: 55%) and cumulative fit (blue).

The IR spectrum of a **Pt⁰Zn^{δ+}/SiO₂** self-supporting pellet exposed to CO (3 mg, 12 mbar) shows an intense CO vibrational band centered at 2046 cm⁻¹ that is red shifted by 38 cm⁻¹ compared to what is observed for Pt particles (2084 cm⁻¹) supported on silica – **Pt⁰/SiO₂** (2.2±0.8 nm) – prepared by a similar approach (grafting of [Pt(OSi(OtBu)₃)₂(COD)] onto SiO₂ followed by a treatment under H₂ at 500 °C). The shift is ascribed to an inherent difference in the particle surfaces of the **Pt⁰/SiO₂** and **Pt⁰Zn^{δ+}/SiO₂** materials attributed to alloy formation of the two components in **Pt⁰Zn^{δ+}/SiO₂** (Figure 2 (a)).²⁶ Additionally, H₂ and CO chemisorption studies also support the inherent difference of the particle surface in **Pt⁰Zn^{δ+}/SiO₂** compared to **Pt⁰/SiO₂** (see supporting information for details). A background subtracted spectrum of **Pt⁰Zn^{δ+}/SiO₂** (12 mg, 120 mbar CO; Figure 2 (b)) shows weak bands at 2202 cm⁻¹ and 2179 cm⁻¹ consistent with CO adsorbed on Zn^{II} sites, similar to those found in **Zn^{II}/SiO₂** (13 mg, 123 mbar CO; 2206

desorption was also used to probe the surface property of the material. Vibrational bands at 1538 cm⁻¹, 1438 cm⁻¹ and 1408 cm⁻¹ are associated with the interaction of pyridine with Pt species on SiO₂ and α-pyridyl species on Pt{111}.^{27,28} Bands at 1610 cm⁻¹ and 1452 cm⁻¹ – similar to **Zn^{II}/SiO₂** – as well as 1595 cm⁻¹ and 1445 cm⁻¹ for **Pt⁰Zn^{δ+}/SiO₂** indicate two different types of Lewis acidic Zn sites – a stronger and a weaker one – on the surface of the material.^{22,29} No bands above 1610 cm⁻¹ indicate a low Brønsted acidity of the support (see supporting information for details).³⁰ The combined results of the CO and pyridine IR studies suggest the formation of an alloyed Pt-Zn material along with residual surface Zn^{II} sites.

XPS was used to gather further insight in the chemical state of Pt and Zn as well as the composition of the material. The results are summed up in **Table 1**. The Pt 4f_{7/2} binding energy in **Pt⁰Zn^{δ+}/SiO₂** is 71.6 eV which is shifted by +0.3 eV compared to **Pt⁰/SiO₂**, likely due to the restructuring of the Pt 4f states upon



alloying with Zn.³¹ The Zn $2p_{3/2}$ peak for $\text{Zn}^{\text{II}}/\text{SiO}_2$ consists of a symmetric component centered at 1023.1 eV (Figure 2 (c)), while the Zn $2p_{3/2}$ peak for $\text{Pt}^0\text{Zn}^{\delta+}/\text{SiO}_2$ (Figure 2 (d)) is asymmetric and was therefore fitted with two components at 1021.7 eV (55% of area) and 1023.1 eV (45% of area). The lower binding energy component can be attributed to Zn^0 (through Zn^{II} reduction). This binding energy is close to the reported value for Zn metal (1021.8(2) eV)³², while the other value parallels what is found for $\text{Zn}^{\text{II}}/\text{SiO}_2$, in accordance with a minority of Zn remaining on the surface as Zn^{II} .

Table 1. XPS $2p_{3/2}$ and $4f_{7/2}$ data of the $\text{Zn}^{\text{II}}/\text{SiO}_2$, Pt^0/SiO_2 and $\text{Pt}^0\text{Zn}^{\delta+}/\text{SiO}_2$ materials.

sample	Zn $2p_{3/2}$ BE [eV]	Pt $4f_{7/2}$ BE [eV]	FWHM $2p_{3/2}$ [eV]	FWHM $4f_{7/2}$ [eV]
$\text{Zn}^{\text{II}}/\text{SiO}_2$	1023.1	-	2.7	-
Pt^0/SiO_2	-	71.3 ^a	-	2.1 ^a
$\text{Pt}^0\text{Zn}^{\delta+}/\text{SiO}_2$	1021.7; 1023.1	71.6	2.0; 3.6	2.1

^a value taken from ²¹.

X-ray absorption studies of the materials have also been performed at the Zn K-edge and Pt L_3 -edge in order to obtain a better understanding of the nature of Pt and Zn in the catalyst precursors and $\text{Pt}^0\text{Zn}^{\delta+}/\text{SiO}_2$. Figure 3 (a) shows the Zn K-edge X-ray absorption near-edge structure (XANES) spectra of $\text{Pt}(\text{OSi}(\text{OtBu})_3)(\text{COD})\text{Zn}^{\text{II}}/\text{SiO}_2$, $\text{Pt}^0\text{Zn}^{\delta+}/\text{SiO}_2$ and Zn foil. An edge shift of -3.8 eV from $\text{Pt}(\text{OSi}(\text{OtBu})_3)(\text{COD})\text{Zn}^{\text{II}}/\text{SiO}_2$ to $\text{Pt}^0\text{Zn}^{\delta+}/\text{SiO}_2$ clearly indicates the reduction of Zn^{II} to Zn^0 . The differences in shape and edge position of $\text{Pt}^0\text{Zn}^{\delta+}/\text{SiO}_2$ compared to Zn foil are attributed to alloy formation of Zn with Pt along with Zn^{II} species as supported by comparison of the derivative spectra of $\text{Pt}(\text{OSi}(\text{OtBu})_3)(\text{COD})\text{Zn}^{\text{II}}/\text{SiO}_2$ and $\text{Pt}^0\text{Zn}^{\delta+}/\text{SiO}_2$ (Figure 3 (b)) revealing the existence of a remaining oxidized Zn species in $\text{Pt}^0\text{Zn}^{\delta+}/\text{SiO}_2$ – in accordance with the observations of adsorption IR studies and XPS – attributed to Zn^{II} sites on the support surface. A linear combination fit of $\text{Pt}(\text{OSi}(\text{OtBu})_3)(\text{COD})\text{Zn}^{\text{II}}/\text{SiO}_2$ and Zn foil

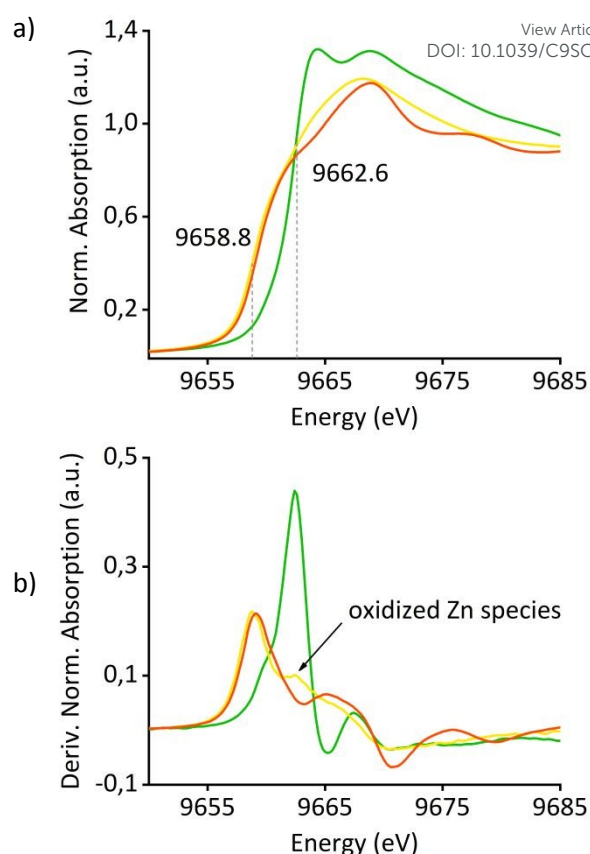


Figure 3. (a) XANES spectra of $\text{Pt}(\text{OSi}(\text{OtBu})_3)(\text{COD})\text{Zn}^{\text{II}}/\text{SiO}_2$ (green), $\text{Pt}^0\text{Zn}^{\delta+}/\text{SiO}_2$ (yellow) and Zn foil (red). (b) First derivative spectra of the same materials.

spectra suggests 22% of Zn remaining as Zn^{II} sites on the surface of $\text{Pt}^0\text{Zn}^{\delta+}/\text{SiO}_2$ (supporting information Figure S21). Analysis of the extended X-ray absorption fine structure (EXAFS) of the Zn K-edge of the material precursors $\text{Pt}(\text{OSi}(\text{OtBu})_3)(\text{COD})\text{Zn}^{\text{II}}/\text{SiO}_2$ and $\text{Zn}^{\text{II}}/\text{SiO}_2$ (see Table 2 and supporting information Figures S24-S27 and Tables S4-S5) reveals a significant elongation of the Zn-O bond distance in the former material compared to the latter, an indication for some changes in the local environment of Zn upon grafting of $\text{Pt}(\text{OSi}(\text{OtBu})_3)_2(\text{COD})$, consistent with the interaction of the Zn^{II} sites with the Pt precursor. In both

Table 2. EXAFS fit parameters of Pt L_3 -edge and Zn K-edge spectra for selected samples^a

sample	neighbor, N ^b	r [Å] ^c	σ^2 [Å ²] ^d
Pt L_3-edge			
$\text{Pt}^0\text{Zn}^{\delta+}/\text{SiO}_2$	Pt, 3.1±1.4	2.62±0.01	0.008±0.002
	Zn, 6.7±2.4	2.48±0.03	0.022±0.004
Pt^0/SiO_2	Pt, 9.1±0.4	2.747±0.002	0.0058±0.0002
Zn K-edge			
$\text{Zn}^{\text{II}}/\text{SiO}_2$	O, 3.5±0.9	1.88±0.02	0.016±0.004
	Si, 0.7±0.6	3.07±0.04	0.005±0.008
$\text{Pt}(\text{OSi}(\text{OtBu})_3)(\text{COD})\text{Zn}^{\text{II}}/\text{SiO}_2$	O, 3.8±0.5	1.94±0.01	0.011±0.002
	Si, 0.7±0.4	3.09±0.02	0.002±0.004

^a samples recorded in transmission mode. ^b Number of specified neighbors. ^c distance to neighbor. ^d Debye-Waller factor.



materials the inclusion of a Zn-Zn instead of a Zn-Si path decreased the fit quality significantly – indicating the high dispersion of Zn^{II} single sites in the precatalyst before the H₂ treatment – also confirmed by a wavelet analysis of [Zn(OSi(OtBu)₃)₂]₂ and Pt(OSi(OtBu)₃)(COD)Zn^{II}/SiO₂ (supporting information Figures S28-S33), clearly showing the disappearance of the Zn-Zn scattering pathway in the latter material. Detailed EXAFS analysis of Pt⁰Zn⁶⁺/SiO₂ was not possible due to the presence of overlapping scattering paths, resulting in fits without physical meaning.

XANES analysis of the Pt L₃ edge of Pt(OSi(OtBu)₃)(COD)Zn^{II}/SiO₂ and Pt⁰Zn⁶⁺/SiO₂ follows similar trends as the Zn K edge (supporting information Figures S33-S34) with a strong decrease in white line intensity upon H₂ treatment – indicating reduction of the corresponding metal – and a shift to lower edge energy, supporting what was observed for the Zn K edge. EXAFS analysis of the Pt L₃ edge of Pt⁰/SiO₂ and Pt⁰Zn⁶⁺/SiO₂ (see Table 2) reveals a considerably shortened Pt-Pt bond distance in the bimetallic material consistent with structural changes and alloy formation. Furthermore, an approximately 2:1 (Zn:Pt) ratio of nearest neighbours for Pt⁰Zn⁶⁺/SiO₂ suggests a 1:1 metal ratio in the nanoparticles (see supporting information for details). However, large errors on the coordination numbers and the fact that XAS only provides average data do not allow the precise determination of particle composition and homogeneity of the alloying. Based on the EA, XPS and XAS results, it can be concluded that Pt⁰Zn⁶⁺/SiO₂ consists of alloyed, PtZn nanoparticles supported on SiO₂ with a fraction of 0.2 to 0.4 of the total Zn remaining as Zn^{II} sites on the surface of the material.

The materials Zn^{II}/SiO₂, Pt⁰/SiO₂ and Pt⁰Zn⁶⁺/SiO₂ were then tested in the PDH reaction at 550 °C under flow conditions (50 ml/min; 20 % C₃H₈ in Ar) in a stainless-steel tubular reactor where negligible mass and heat transfer limitations occur (see calculations in supporting information). The results are summarized in Table 3. A very high initial productivity 703 g_{C₃H₆} g_{Pt}⁻¹ h⁻¹ with a conversion of 30.2 % and selectivity of 98.1 % to C₃H₆ could be achieved for Pt⁰Zn⁶⁺/SiO₂ at a WHSV of 75 h⁻¹. The high selectivity could be maintained over the course of 30 h time on stream with a final selectivity of 95.0 % while the conversion dropped to a final 16.1 % conversion (*k_d* = 0.027 h⁻¹ – see equation (1)) and a productivity of 375 g_{C₃H₆} g_{Pt}⁻¹ h⁻¹.

$$k_d = \frac{\left(\ln \left(\frac{1 - conv_{end}}{conv_{end}} \right) - \ln \left(\frac{1 - conv_{start}}{conv_{start}} \right) \right)}{t} \quad (1)$$



Catalytic tests at lower WHSV of 32 h⁻¹ showed a significant increase in the initial conversion up to 35.3 %, while maintaining high selectivity (>96%) and an almost closed carbon balance (97%). In contrast, **Pt⁰/SiO₂** shows a very low initial productivity (14.5 g_{C₃H₆} g_{Pt}⁻¹ h⁻¹) and a high deactivation rate ($k_d = 0.26$) over the course of 2 h, while **Zn^{II}/SiO₂** shows comparable catalytic performance to **SiO₂₋₇₀₀** (1.2 % conversion, 39-38 % selectivity over 10 h) revealing the absence of catalytic activity of **Zn^{II}/SiO₂** under these conditions.

Comparison of **Pt⁰Zn^{δ+}/SiO₂** to the monometallic **Pt⁰/SiO₂** shows a dramatic improvement in the productivity of the bimetallic system by more than one order of magnitude. Comparison of **Pt⁰Zn^{δ+}/SiO₂** to other Pt/Zn systems reveals superior stability of the reported system (supporting information Table S9). While most systems show high selectivity and conversion levels, significantly larger deactivation factors are observed in comparison to **Pt⁰Zn^{δ+}/SiO₂** or the studies include H₂ co-feeding³³ and significantly lower weight hourly space velocities to decrease deactivation rates. Furthermore, the metal based productivity and the stability of the reported system also surpass these of the recently published Pt/Ga based system (661 (357 after 20 h) g_{C₃H₆} g_{Pt}⁻¹ h⁻¹; $k_d = 0.041$ h⁻¹) prepared via the same SOMC/TMP approach.²¹

To further investigate the structural stability of **Pt⁰Zn^{δ+}/SiO₂** under PDH conditions *in-situ* XAS studies were performed under the same conditions as the catalytic tests. The spectra of **Pt⁰Zn^{δ+}/SiO₂** and **Pt⁰/SiO₂** show no significant change at the Pt L₃ edge over 8h and 2h, respectively. The Zn K edge spectra of **Pt⁰Zn^{δ+}/SiO₂** show a slight and consistent shift over 8 h, indicating a slight structural change for Zn. Preliminary analysis indicates the further – but not complete – reduction of Zn^{II} sites to Zn⁰ (supporting information Figures S48-S49).

The very high productivity of the reported **Pt⁰Zn^{δ+}/SiO₂** system compared to most other Pt/Zn systems is attributed to the formation of subnanometric alloyed particles, probably a result of the high metal dispersion in the precatalyst before reduction. These particles show minor growth during catalysis

over 30 h as shown by post-catalysis TEM analysis (supporting information Figure S8). The narrow particle size distribution and the presence of remaining Lewis acidic Zn^{II} sites on the materials surface could both play a significant role in stabilizing this catalyst. Post-catalysis characterization shows the formation of coke as well as minor particle growth (supporting information Figure S8 and S54), which both are most likely contributing to catalyst deactivation.

Conclusions

This work shows that utilizing SOMC/TMP as a synthetic methodology enables the formation of narrowly distributed bimetallic Pt-Zn subnanometric particles supported on SiO₂. The resulting high productivity and stability in the PDH reaction for the tested range of WHSV compared to other Pt-Zn systems are attributed to the combination of alloying and high metal dispersion. Furthermore, the remaining Zn^{II} surface sites likely play a role to prevent sintering. SOMC/TMP is a unique synthetic tool to address the origin of catalytic performances in complex multi-metallic systems, where composition, size and support effects can play a crucial role; we are currently further investigating this approach as a general tool for the synthesis of model catalysts to establish detailed structure-activity relationships.

Acknowledgements

L. R. thanks the Swiss National Science Foundation (SNSF fond number: 200021_169134) for funding. We thank Dmitry Lebedev and ScopeM for help with TEM measurements. Fabian Müller and Debora Thöny are acknowledged for help with TGA measurements. Ka Wing Chan is thanked for help with XAS interpretation. Scott Docherty is acknowledged for help with chemisorption measurements. Dr. Gina Noh, David Trummer, Petr Šot and Scott Docherty are acknowledged for discussions.

Table 3. Catalytic Performance of **Pt⁰Zn^{δ+}/SiO₂**, **Pt⁰/SiO₂** and **Zn^{II}/SiO₂** at 550 °C under Flow Conditions.^a

sample	Time [h]	Conversion [%]	Selectivity [%] ^b	Carbon balance [%]	Productivity [g _{C₃H₆} / g _{Pt} h]	WHSV [h ⁻¹]	k_d^c [h ⁻¹]
Pt⁰/SiO₂	0.1	2.5	74.9	>99	14.5	32	0.26
	2	1.5	47.1		8.7		
Zn^{II}/SiO₂	0.1	0.9	43.3	>99	-	32	0
	10	0.9	39.6		-		
Pt⁰Zn^{δ+}/SiO₂	0.1	35.3	97.6	97	350	32	0.014
	30	26.6	96.3		264		
Pt⁰Zn^{δ+}/SiO₂	0.1	30.2	98.1	97	703	75	0.027
	30	16.1	95.0		375		

^a 50 ml/min, 20 % C₃H₈ in Ar. ^b selectivity for C₃H₆, only volatile compounds taken into account. ^c $k_d = (\ln((1 - \text{conv}_{\text{end}})/\text{conv}_{\text{end}}) - \ln((1 - \text{conv}_{\text{start}})/\text{conv}_{\text{start}}))/t$.



The whole Copéret group is acknowledged for help with XAS measurements.

References

- J. S. Plotkin, The Propylene Gap: How Can It Be Filled? - American Chemical Society, <https://www.acs.org/content/acs/en/pressroom/cutting-edge-chemistry/the-propylene-gap-how-can-it-be-filled.html>, (accessed 1 November 2019).
- J. S. Plotkin, The Propylene Quandary - American Chemical Society, <https://www.acs.org/content/acs/en/pressroom/cutting-edge-chemistry/the-propylene-quandary.html>, (accessed 1 November 2019).
- J. J. H. B. Sattler, J. Ruiz-Martinez, E. Santillan-Jimenez and B. M. Weckhuysen, *Chem. Rev.*, 2014, **114**, 10613–10653.
- J. Liu, W. Zhou, D. Jiang, W. Wu, C. Miao, Y. Wang and X. Ma, *Ind. Eng. Chem. Res.*, 2018, **57**, 11265–11270.
- Z. Han, S. Li, F. Jiang, T. Wang, X. Ma and J. Gong, *Nanoscale*, 2014, **6**, 10000–10008.
- E. C. Wegener, Z. Wu, H.-T. Tseng, J. R. Gallagher, Y. Ren, R. E. Diaz, F. H. Ribeiro and J. T. Miller, *Catal. Today*, 2018, **299**, 146–153.
- J. J. H. B. Sattler, I. D. Gonzalez-Jimenez, L. Luo, B. A. Stears, A. Malek, D. G. Barton, B. A. Kilos, M. P. Kaminsky, T. W. G. M. Verhoeven, E. J. Koers, M. Baldus and B. M. Weckhuysen, *Angew. Chemie Int. Ed.*, 2014, **53**, 9251–9256.
- Q. Zhang, K. Zhang, S. Zhang, Q. Liu, L. Chen, X. Li, C. Wang and L. Ma, *J. Catal.*, 2018, **368**, 79–88.
- J. T. Miller, V. J. Cybulska, B. C. Bukowski, H.-T. Tseng, J. R. Gallagher, Z. Wu, E. Wegener, A. J. Kropf, B. Ravel, F. H. Ribeiro and J. Greeley, *ACS Catal.*, 2017, **7**, 4173–4181.
- Z. Nawaz, *Rev. Chem. Eng.*, 2015, **31**, 413–436.
- Y. Zhang, Y. Zhou, L. Huang, S. Zhou, X. Sheng, Q. Wang and C. Zhang, *Chem. Eng. J.*, 2015, **270**, 352–361.
- G. Liu, L. Zeng, Z.-J. Zhao, H. Tian, T. Wu and J. Gong, *ACS Catal.*, 2016, **6**, 2158–2162.
- C. Copéret, A. Comas-Vives, M. P. Conley, D. P. Estes, A. Fedorov, V. Mougel, H. Nagae, F. Núñez-Zarur and P. A. Zhizhko, *Chem. Rev.*, 2016, **116**, 323–421.
- M. K. Samantaray, E. Pump, A. Bendjeriou-Sedjerari, V. D'Elia, J. D. A. Pelletier, M. Guidotti, R. Psaro and J.-M. Basset, *Chem. Soc. Rev.*, 2018, **47**, 8403–8437.
- M. M. Stalzer, M. Delferro and T. J. Marks, *Catal. Letters*, 2015, **145**, 3–14.
- K. L. Fujdala and T. D. Tilley, *J. Catal.*, 2003, **216**, 265–275.
- C. Copéret, *Acc. Chem. Res.*, 2019, **52**, 1697–1708.
- K. Larmier, W.-C. Liao, S. Tada, E. Lam, R. Verel, A. Bansode, A. Urakawa, A. Comas-Vives and C. Copéret, *Angew. Chemie Int. Ed.*, 2017, **56**, 2318–2323.
- E. Lam, K. Larmier, P. Wolf, S. Tada, O. V. Safonova and C. Copéret, *J. Am. Chem. Soc.*, 2018, **140**, 10530–10535.
- G. Noh, E. Lam, J. L. Alfke, K. Larmier, K. Searles, P. Wolf and C. Copéret, *ChemSusChem*, 2019, **12**, 968–972.
- K. Searles, K. W. Chan, J. A. Mendes Burak, D. Zemlyanov, O. Safonova and C. Copéret, *J. Am. Chem. Soc.*, 2018, **140**, 11674–11679. DOI: 10.1039/C9SC05599A
- A. K. Cook and C. Copéret, *Organometallics*, 2018, **37**, 1342–1345.
- N. Rendón, A. Bourdolle, P. L. Baldeck, H. Le Bozec, C. Andraud, S. Brasselet, C. Coperet and O. Maury, *Chem. Mater.*, 2011, **23**, 3228–3236.
- P. Laurent, L. Veyre, C. Thieuleux, S. Donet and C. Copéret, *Dalt. Trans.*, 2013, **42**, 238–248.
- D. A. Ruddy, J. Jarupatrakorn, R. M. Rioux, J. T. Miller, M. J. McMurdo, J. L. McBee, K. A. Tupper and T. D. Tilley, *Chem. Mater.*, 2008, **20**, 6517–6527.
- A. G. T. M. Bastein, F. J. C. M. Toolenaar and V. Ponc, *J. Catal.*, 1984, **90**, 88–95.
- B. A. Morrow, I. A. Cody, L. E. Moran and R. Palepu, *J. Catal.*, 1976, **44**, 467–476.
- S. Haq and D. A. King, *J. Phys. Chem.*, 1996, **100**, 16957–16965.
- C. Morterra and G. Cerrato, *Catal. Letters*, 1991, **10**, 357–363.
- R. Ferwerda, J. H. van der Maas and F. B. van Duijneveldt, *J. Mol. Catal. A Chem.*, 1996, **104**, 319–328.
- J. A. Rodriguez and M. Kuhn, *J. Chem. Phys.*, 1995, **102**, 4279–4289.
- S. P. Kowalczyk, R. A. Pollak, F. R. McFeely, L. Ley and D. A. Shirley, *Phys. Rev. B*, 1973, **8**, 2387–2391.
- V. Galvita, G. Siddiqi, P. Sun and A. T. Bell, *J. Catal.*, 2010, **271**, 209–219.

